Uplift Pressures below Spillway Chute Slabs at Unvented Open Offset Joints

Tony L. Wahl, P.E., M.ASCE[1]; K. Warren Frizell[2]; and Henry T. Falvey, Dr.Eng., D.WRE, M.ASCE[3]

Abstract: The catastrophic failure of the spillway chute at Oroville Dam in February 2017 raised concerns throughout the water resources industry regarding design, construction, and maintenance practices for concrete spillway chutes, especially joints and cracks that could allow penetration of high-pressure water into a chute foundation. The independent forensic team investigation found that hydraulic jacking was the most likely cause of the initial chute slab failure, highlighting a need for better analysis of the hydraulic jacking potential of existing spillways and more resilient designs for spillways that operate under high-velocity flow conditions. This paper reviews the Oroville Dam event and findings and previous laboratory testing performed to evaluate uplift pressures and flow transmitted through spillway joints. A reanalysis of previous studies was used to develop relations between chute velocity, joint geometry, and uplift pressure transmitted into a joint. Uplift pressure head in these relations is expressed in a dimensionless manner, either as a percentage of the velocity head in the boundary layer at midheight of the offset into the flow, or as a percentage of the channel-average velocity head. The first approach is potentially more useful for prototype applications, but the second method provides the best fit to the available experimental data. Additional research is still needed to quantify rates of flow through open joints, confirm relations between uplift pressure and boundary layer velocities, and evaluate the effects of aerated flow. **DOI: 10.1061/(ASCE)HY.1943-7900.0001637.**

Introduction

The February 2017 failure of the spillway chute at Oroville Dam, owned and operated by the California Department of Water Resources (DWR), raises significant concerns about aging spillway structures. As dams and spillways age, concrete surfaces and masses slowly deteriorate, slabs may shift because of foundation settlement or frost heave, reinforcement bars and anchors may corrode and lose strength, and auxiliary components such as underslab drain systems can be compromised by sediment deposition, scour, and intrusion of tree roots. Once concrete surfaces suffer initial deterioration, other problems become more likely, including cavitation damage, increased uplift forces at joints, and acceleration of deterioration rates due to freeze-thaw action.

One of the most likely locations for problems to occur in a concrete spillway chute is at or near the joints. Common types of joints include construction joints, control joints, expansion joints, and contraction joints. Joints typically deteriorate faster than slabs, and they offer opportunities for surface offsets and entry of pressurized flow into foundation areas, key elements for cavitation and hydraulic jacking failure modes. Even if uplift pressures are not large enough to cause immediate slab movement, the flows that enter the foundation through open joints can cause erosion and the development of voids beneath slabs that may ultimately lead to slab movement, offsetting of joints, and uplift.

Despite their problems, joints are a practical necessity because spillways are large structures that typically must be constructed in a specific sequence and in multiple phases over several months or years. Joints placed at regular intervals enable staged construction, permit thermal contraction and expansion, and help to control cracks in the finished product. The geometry and construction details of joints vary, which affects their vulnerability to uplift and seepage flow. Although modern design standards for spillway joints (e.g., Bureau of Reclamation 2014) include details meant to prevent the development of offsets and gaps (e.g., keys, structural reinforcement) and limit flow through joints (waterstops), older spillways like Oroville lack some or all of these features or have other deficiencies (e.g., poorly prepared foundations, inadequate or deteriorated drainage systems) that make them vulnerable to uplift failures.

Hydraulic jacking occurs when the forces acting to lift a spillway slab exceed the forces resisting upward movement. Resisting forces include the weight of the slab itself, the capacity of foundation anchors, and the pressure applied to the top of the slab by water flowing in the chute. Uplift can be created through a combination of increased pressure below the slab and reduced pressure above the slab (i.e., lift). High pressures can be generated below a slab when high-velocity flow stagnates against an offset into the flow at a joint that is open to the foundation. Offsets can occur due to settlement of an upstream slab or lifting or tilting of the edge of a downstream slab, or with no slab movement when the concrete surface is spalled upstream from a joint. Slab movements that lead to offsets may occur because of drying or wetting of soil foundations, frost heave, or internal erosion of foundation soils when flow through open joints is not captured or retained within a drainage system. When internal erosion leads to the development of large voids beneath a slab, this may enable high pressures generated at a joint to more readily act over a large area beneath the slab.

Lift on the top surface of a slab can occur because of gradual curvature of the spillway surface away from the flow, or abrupt separations of flow from the spillway surface. Steps up or down caused by misalignment of joints are capable of generating localized

[1]Technical Specialist, Bureau of Reclamation, Hydraulic Investigations and Laboratory Services, Denver, CO 80225-0007 (corresponding author). ORCID: https://orcid.org/0000-0002-2081-2263. Email: twahl@usbr.gov

[2]Retired; formerly, Hydraulic Engineer, Bureau of Reclamation, Hydraulic Investigations and Laboratory Services, Denver, CO 80225-0007.

[3]Consultant, Henry T. Falvey & Associates, 11624 Blackfoot Rd., Conifer, CO 80433.

Note. This manuscript was submitted on October 5, 2018; approved on March 22, 2019; published online on September 13, 2019. Discussion period open until February 13, 2020; separate discussions must be submitted for individual papers. This paper is part of the ***Journal of Hydraulic Engineering***, © ASCE, ISSN 0733-9429.

low-pressure zones. Dong et al. (2010) studied cavitation at offsets into the flow and measured negative pressures approaching the vapor pressure of water in the separation zone downstream from 2- and 5-mm-high offsets, but pressure recovery was also observed to begin 75–100 mm downstream. Vapor pressure establishes the minimum possible pressure on the upper surface of a spillway slab, limiting the contribution of flow separation to the uplift head to about 10 m (33 ft), but stagnation pressure heads associated with high-velocity flow can be much larger. For example, the stagnation pressure associated with a velocity of 30 m/s (98 ft/s) is about 46 m (151 ft). For this reason, most analyses of uplift forces have focused on the pressure increase beneath the slab. In previous experimental work to be discussed later in this paper, the reported uplift was the net difference between the increased pressure below the slab and the pressure above the slab associated with a relatively shallow flow depth.

Additional factors that may be important in spillway slab uplift are air entrained in the flow above the slab and its effect on pressures generated within the joints, and the role of fluctuating pressures in combination with steady uplift. These two factors may also be linked to some degree, as Bollaert and Schleiss (2003a, b) showed that air is an important factor in creating a resonance effect that magnifies pressure fluctuations within closed-end fissures in fractured rock masses.

Hepler and Johnson (1988) and Trojanowski (2004) documented hydraulic jacking failures in Bureau of Reclamation spillways at Dickinson Dam (North Dakota) in 1954 and at Big Sandy Dam (Wyoming) in 1983. At Dickinson Dam, there was a lack of defensive design features such as foundation grouting, anchor bars, and waterstops, and the underdrain system was compromised by subfreezing temperatures. In addition, there were several possible mechanisms that could have led to joints with offsets and openings that permitted pressurized flow to enter the foundation. Unfiltered gravel zones around the underdrain system were also implicated as a factor in internal erosion that led to the development of voids beneath the slabs. At Big Sandy Dam, freezing temperatures over many years caused deterioration of the spillway concrete, damage to the underdrain system, and slab movement that produced open and offset joints. Uplift pressures at the time of failure were large enough to pull the foundation rock anchors out of the soft sandstone foundation [1.2-m (4-ft)–long, 25-mm (1-in.)–diameter bars on 1.5-m (5-ft) centers, with a design capacity of 44 kN (10 kips) each]. It was speculated that the anchors may have been only 50% effective because of deterioration of the grout-foundation contact and could have been failed by an uplift pressure head greater than 49% of the mean velocity head, which was a feasible failure scenario (Trojanowski 2004). Considering these failures and experiences from other spillways exhibiting various types of distress, Trojanowski (2008) discussed the evaluation of potential failure modes of spillways, including factors related to hydraulic jacking.

Oroville Dam Spillway Failure

The description of the Oroville Dam spillway chute failure given in this section is summarized from the report of the Oroville Dam Independent Forensic Team (IFT 2018).

Oroville Dam is an embankment dam located on the Feather River in northern California—the tallest dam in the United States at 235 m (770 ft). The dam is owned and operated by DWR, which was responsible for design and construction, completed in 1968. It is one component of the Oroville-Thermalito Complex, which includes several hydroelectric powerplants, canals, and diversion and fish barrier dams. The complex is a major feature of the California State Water Project, the largest state-owned water storage and delivery system in the United States. On February 7, 2017, the service spillway chute lining failed, leading to an emergency that lasted for several weeks while the spillway was required to continue operating.

At the time of the failure, Oroville Dam was equipped with two spillways. The gated spillway, described as the service spillway or flood control outlet (FCO), was controlled by eight large top-seal radial gates and discharged into a concrete chute that was 54.5 m (178.67 ft) wide and 914 m (3,000 ft) long. The emergency spillway, which had never operated, was a 518-m (1,700-ft)–long uncontrolled overflow weir discharging into an unimproved steep natural drainage leading back to the Feather River. The service spillway chute was originally designed for a maximum flow rate of 7,080 m^3/s (250,000 ft^3/s). The historical maximum instantaneous discharge was 4,530 m^3/s (160,000 ft^3/s) in 1997, about 64% of the design discharge (IFT 2018). The spillway had operated infrequently in its 49-year history, with about 4 days of operation above 2,830 m^3/s (100,000 ft^3/s), 40 days above 2,120 m^3/s (60,000 ft^3/s), and 300 days above 1,060 m^3/s (30,000 ft^3/s). Soon after construction was completed, cracking of the spillway slab occurred over embedded drain pipes, which were arranged in a herringbone pattern down the length of the spillway. As result, there was a long history of periodic repairs made to maintain the service spillway chute slab.

Due to heavy snow and rain in northern California in the winter of 2016–2017, the service spillway operated for about five days in mid-January 2017 at flow rates up to about 283 m^3/s (10,000 ft^3/s)—the first significant flows since 2011. The spillway was shut down around January 20 and then restarted around February 1. Discharges were gradually increased during early February. At about 10:10 a.m. on the morning of February 7, while the discharge was being increased from 1,200 to 1,490 m^3/s (42,500 to 52,500 ft^3/s), DWR personnel working near the left side of the service spillway chute heard a loud sound they compared to an explosion. They subsequently observed spray and significantly disturbed flow conditions in the spillway chute near Station 1,020 m (33 + 50 ft), about 640 m (2,100 ft) downstream from the spillway radial gates. The spillway continued to operate for about one hour, and then, from about 11:25 a.m. to 12:25 p.m. the spillway gates were closed, revealing the damage shown in Fig. 1.

Because of forecasted large inflows, a continued need for spillway operations was anticipated. Following initial damage assessments and release of some closely monitored test flows, the

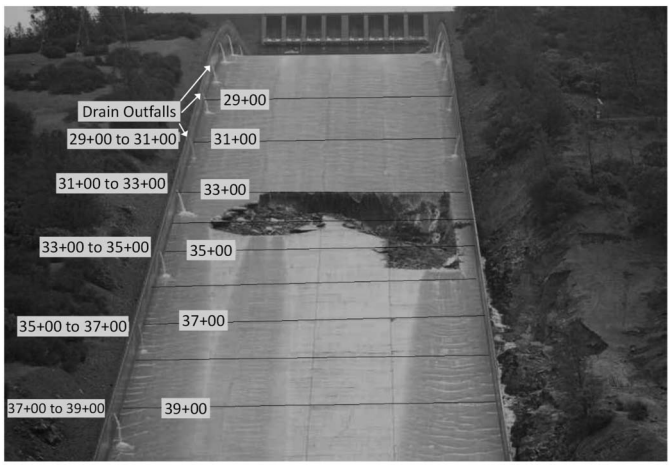

Fig. 1. Spillway damage observed after gates were initially closed at midday, February 7, 2017. (Reprinted from IFT 2018, with permission.)

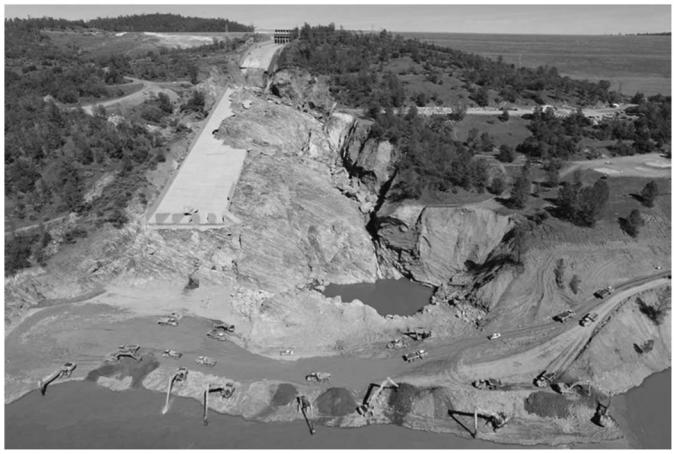

Fig. 2. Ultimate damage at the Oroville Dam service spillway in May 2017. (Reprinted from IFT 2018, with permission.)

spillway was placed back into service from February 8 to February 10 at discharges up to 1,840 m^3/s (65,000 ft^3/s), with erosion and damage to the chute structure continuing. Unfortunately, these releases were not enough to keep up with inflow to the reservoir. Early on February 11, the reservoir level exceeded Elevation 274.62 m (901 ft) and the emergency spillway began to flow for the first time in its history. The reservoir level eventually reached Elevation 275.11 m (902.59 ft) at about 3:00 a.m. on February 12, with a peak flow of about 354 m^3/s (12,500 ft^3/s) over the emergency spillway crest. There was extensive erosion and headcutting in the natural channel below the emergency spillway crest, and headcuts advancing upstream toward the spillway crest threatened its stability. At 3:35 p.m. on February 12, the service spillway gate openings were increased to draw the reservoir down and reduce flows over the emergency spillway crest. At 3:44 pm on February 12, an evacuation order was issued for about 188,000 downstream residents because of rapidly progressing erosion in the emergency spillway discharge channel. The service spillway flows reached 2,830 m^3/s (100,000 ft^3/s) by about 7:00 p.m. on February 12 and were maintained there for about 3.5 days through 8:00 a.m. on February 16. During this period, reservoir levels dropped significantly and the situation stabilized. Service spillway flows were gradually reduced over subsequent days until the spillway was shut down again on February 27. After new inspections, the service spillway was placed back into operation in early March and operations continued until it was shut down for the season on May 19. The damage to the spillway at the end of the operating season is shown in Fig. 2.

Forensic Investigation

A six-member independent forensic team (IFT) (including the third author) was formed after the Oroville Dam spillway slab failure, with the following charge:

> To complete a thorough review of available information to develop findings and opinions on the chain of conditions, actions, and inactions that caused the damage to the service spillway and emergency spillway, and why opportunities for intervention in the chain of conditions, actions, or inactions may not have been realized.

Their report issued in January 2018 provides the IFT's opinion on the physics of the failure process and the most likely failure modes. The report also identifies physical factors and features of the design that contributed to the failure and identifies organizational and human factors that contributed to the failure and affected the response to the emergency.

The IFT concluded that the spillway chute failure most likely was initiated by uplift and removal (hydraulic jacking) of a section of the chute slab near Station 1,020 m (33 + 50 ft), just downstream from the end of the vertical curve in the chute that transitions from a 5.67% slope to a 24.5% slope. High-velocity flow then rapidly eroded moderately to highly weathered rock and soil-like foundation materials beneath adjacent slabs. The initial uplift failure was believed to have affected only part of one of the 12.2 × 15.2-m (40 × 50-ft) chute slab panels, and could have removed something as small as a localized repair patch or a spall above a drain, or as large as a 6-m (20-ft) section located between cracks that existed above the herringbone drains partially embedded in the bottom of the slab. Once the initial portion of the slab failed, it probably triggered a rapid chain of subsequent events, leading to additional slab section failures (IFT 2018).

The IFT report discussed the possibility of an initial failure due to sagging or settling of a slab into an underlying void. The team could not absolutely rule out this possibility, but found it less likely than an uplift failure for several reasons, including the suddenness of the failure, eyewitness reports of explosion-like sounds, and a lack of any evidence of sagging in photos taken of the spillway after the operations in early January 2017. The team also allowed for the possibility that localized settlement upstream from a joint or crack could have created an offset into the flow that led to injection of high-pressure water beneath the slab downstream from that location.

Contributing Factors

Several physical factors were cited by the IFT that contributed to the initial failure and subsequent damage to the spillway chute. Although the team was confident that the initial failure occurred because of uplift created by high-velocity flow being injected through a feature of some kind in the chute slab surface, they could not pinpoint the specific type or exact location of the feature. Possibilities they listed included open joints, unsealed cracks over lateral drainage pipes (the herringbone drains), spalled concrete at either a joint or a drain location in a new or previously repaired area, or some combination of multiple features. The IFT made calculations of potential discharges through cracks and joints and believed that the flows could have far exceeded the localized capacity of the drain system, causing flow to back up in the drains and increase uplift forces.

Several contributing factors were specifically listed by the IFT as possible explanations for why the spillway chute failed in 2017 at a discharge of about 1,490 m^3/s (52,500 ft^3/s), but had not failed in earlier high-flow events, such as a release of more than 1,980 m^3/s (70,000 ft^3/s) in 2006 and the maximum discharge of 4,530 m^3/s (160,000 ft^3/s) in 1997. All of these contributing factors are related to slow changes in the condition of the spillway materials or foundation over time.

- New chute slab damage and/or deterioration of previous slab repairs.
- Expansion of relatively shallow void(s) under the slab, through erosion or shrinkage of clay soils.
- Corrosion of steel reinforcing bars or dowels across the concrete cracks or joints.
- Reduction in anchor capacity.

Hydraulic Analyses

Appendix B of the IFT's report provided detailed analysis and discussion of hydraulic phenomena that were considered by the team in connection with their efforts to identify the initiating cause of failure and contributing factors.

Stagnation and Uplift Pressures

To evaluate the potential uplift pressures that could act on a spillway slab, the IFT report described an approach to estimating the stagnation pressure that could occur at a vertical offset into the flow. When flow strikes the face of such an offset, it is deflected downward into the joint and up and over the offset. At the dividing line between these flows, the flow stagnates against the face of the offset and its kinetic energy is converted into potential energy in the form of pressure head—*stagnation pressure*. With an opening in the joint, all or a portion of the stagnation pressure can be transmitted through the joint, creating uplift beneath the slab. Stagnation pressure can also drive flow into the joint, and this flow must be carried away by the drainage system beneath the slab to avoid a buildup of pressure.

In a prototype spillway with a long chute, a velocity profile develops in the chute with low velocities near the bed and high velocities near the water surface. The greatest variation of velocities occurs very near the bed in the boundary layer. At a significant distance down the chute, the thickness of the boundary layer could be enough for offsets at spillway joints to be contained entirely within the boundary layer. In this case, flow offsets would be exposed to velocities that are lower than the average velocity within the whole channel. Referring to a study of flow over open offset joints by Frizell (2007) that used particle image velocimetry (PIV) to map velocity fields approaching a joint, the IFT report suggested that the streamline of the flow stagnating against the face of an offset into the flow tended to be located at about half of the offset height. With the failure taking place about 640 m (2,100 ft) downstream from the control gates, the boundary layer was estimated to have a thickness of about 1 m (3.3 ft), with a well-developed velocity profile in the channel. To estimate the velocity at various heights above the channel floor that might correspond to the midheight of offsets of different sizes, the IFT used an equation provided by Rouse [1945, p. 199, Eq. (157)] to describe the velocity profile versus depth in an open channel flow:

$$\frac{v_y - V}{V\sqrt{f}} = 2\log_{10}\frac{y}{y_0} + 0.88 \tag{1}$$

where v_y = velocity at distance y above the boundary; f = Darcy-Weisbach friction factor; y = distance from the boundary; y_0 = total flow depth; and V = mean flow velocity.

It is important to note that y_0 is the total flow depth and that Eq. (1) computes an estimate of the entire velocity profile from the boundary to the free surface, not just the velocity within the boundary layer near the bed. (The IFT report incorrectly identified y_0 as the depth where the velocity is zero.) This equation is sensitive to surface roughness through the friction factor, f, so rougher surfaces have a more pronounced velocity profile with lower velocities near the channel bed. Once v_y is estimated, the associated stagnation pressure is

$$\frac{P_s}{\gamma} = \frac{v_y^2}{2g} \tag{2}$$

where P_s = stagnation pressure; γ = unit weight of water; v_y = approach velocity of the stagnated flow; g = acceleration due to gravity.

Table 1 shows stagnation pressures estimated at 50% of the offset height for two flow rates and three joint offset heights. The two flow rates bracket the conditions at the time of the initial Oroville failure, and the flow depths and velocities at the station of the failure are determined from water surface profile calculations (Falvey 1990; Wahl et al. 2019), assuming a surface roughness of 0.3 mm (0.001 ft). This table is similar to Table 2 in Appendix B of the IFT report, but corrects three problems that affected that table: (1) velocities were calculated at the tip of the offset, even though the text of the IFT report said they were calculated at the midheight; (2) stagnation pressure head values were actually velocities that had not yet been converted to pressure head; and (3) incorrect friction factors were used that were much too large. For Table 1 here, friction factors were determined with the Colebrook-White equation as an integral part of the water surface profile calculations. In this particular example, the combined corrections for these three problems largely offset one another, so the numerical stagnation pressure head values in Table 1 are not dramatically different from those given in the IFT report.

The stagnation pressures shown in Table 1 can become the source for generating uplift pressure beneath a slab, but the IFT report emphasized that there was uncertainty regarding the extent over which the uplift force would act. The type of drain system beneath the joint or the porosity and permeability of soils beneath the joint would affect the distribution and extent of uplift pressures. The IFT report did not estimate a probable pressure distribution or total uplift force on a whole slab or portion of a slab, but used the analysis only to show the magnitude of uplift pressures that could have been generated and the trends for increasing uplift pressure with increasing discharge. The stagnation pressure head increases 22% when the flow rate increases 80% from 850 to 1,530 m^3/s (30,000 to 54,000 ft^3/s). Note that the estimated stagnation pressures are small fractions (30%–50%) of the total velocity head of the mean flow, which illustrates the significant effect of basing the stagnation pressure estimates on the velocity near the surface, rather than on the mean channel velocity. This analysis is sensitive to the assumed hydraulic roughness of the flow surface. With increased roughness the calculated stagnation pressures drop significantly and there is greater sensitivity to the offset height.

Table 1. Stagnation pressures at Station 1,006 m (33 + 00 ft) of the Oroville Dam spillway, at half of offset height for three hypothetical offsets

Discharge (m^3/s)	Flow depth (m)	Average velocity (m/s)	Average velocity head (m)	Darcy-Weisbach friction factor, f	Stagnation pressure head at 50% of offset height (m) (and as percentage of channel-average velocity head)		
					6-mm offset	12-mm offset	25-mm offset
850	0.60	26.1	34.6	0.0132	11.3 (33%)	14.3 (41%)	17.7 (51%)
1,530	0.94	30.0	46.0	0.0121	13.8 (30%)	17.3 (38%)	21.5 (47%)

Source: Adapted from IFT (2018, Appendix B, Table 2).
Note: Errors in the original table are corrected and pressures are provided in SI units and as percentages of channel-average velocity head.

The analytical approach taken by the IFT depended on some significant assumptions. For a given joint offset height, the uplift pressure was estimated by assuming that stagnation of the velocity occurs at 50% of the offset height, and that 100% of this stagnation pressure was transmitted through the joint. Each of these assumptions should be verified with either lab or field testing. In addition, to apply this analysis to the practical problem of determining net uplift force, the drainage system and/or underlying foundation must be analyzed to determine how drainage will dissipate the uplift pressure. Once the resulting uplift forces are estimated, the design of the slab and its anchorage can be evaluated to determine if the slab can withstand the applied loads.

Flow through Joints or Cracks

The IFT report analyzed the potential for seepage or leakage flow through open spillway joints or cracks. The analysis used the energy equation applied to the slot behaving as a pressurized conduit experiencing turbulent flow. It considered only joints and cracks that were flush, with no offset into or away from the flow. The driving force for flow through the joint was only the hydrostatic pressure associated with the spillway flow depth, not any stagnation pressure. No quantitative estimates were made of the density of cracking in the slab or the prevalence of open joints, but the IFT found that the drainage system beneath the Oroville Dam spillway chute would have been unable to convey the volume of flow that might have come from the widespread open joints or cracks.

The analysis performed by the IFT did not consider the increased flow through a joint that could occur because of stagnation pressure developing against the entrance to an offset joint. Laboratory testing has not yet provided reliable information that can be used for this purpose.

Previous Research

Despite historical cases of spillway chute slab failure by hydraulic jacking, efforts to quantify the uplift pressures generated by high-velocity flows over offset and open spillway joints have been very limited. Most studies of uplift have focused on slabs and joints in stilling basins and plunge pools, where fluctuating pressures generated by hydraulic jumps and impinging jets are the driving mechanism (Toso and Bowers 1988; Fiorotto and Rinaldo 1992a, b; Bellin and Fiorotto 1995; Fiorotto and Salandin 2000; Melo et al. 2006; Liu and Li 2007; Mahzari and Schleiss 2010; González-Betancourt and Posada-García 2016). Bowers and Toso (1988) described a model study intended to investigate this mechanism in the failure of one specific spillway stilling basin. Fiorotto and Caroni (2014) and Barjastehmaleki et al. (2016a, b) considered how the high pressures generated at stilling basin slab joints propagate beneath the slab and dissipate with increasing distance from the joint.

High pressures generated in the joints and cracks of rock masses have also been studied extensively as a driving mechanism for scour in rocky plunge pools and unlined rock channels (Bollaert and Schleiss 2005; Pells 2016), but not with a focus on joints with the regularity or extent of those found in concrete spillway linings. Most of this work has been directed toward the prediction of removal of individual rock blocks or the breakup of large rock masses into smaller units due to intense pressure fluctuations on rock surfaces or within joints. Key features of the flows driving these processes are impingement of jets at angles ranging from normal to acute, aeration and disintegration of jets both above and below the water level of the pool, and sizable pressure fluctuations applied to slab surfaces and joints. These characteristics stand in sharp contrast to gradually varied flows that are essentially parallel to relatively smooth spillway chutes. The flume study by Pells (2016) produced measurements of pressure generated within the joints surrounding an idealized rock block projecting into a high-velocity open-channel flow similar to that in a spillway chute, but included many three-dimensional effects that would be absent or much different for flow over a typical chute slab joint.

To the authors' knowledge, the only studies of uplift pressure due to unidirectional high-velocity flow over offset spillway joints are those of Johnson (1976) and Frizell (2007), both conducted in the Hydraulics Laboratory of the Bureau of Reclamation. Those two studies are reviewed here and the data further analyzed with a view toward application to situations like the event at Oroville Dam.

Open-Channel Tests

Johnson (1976) studied uplift pressures beneath spillway chute slabs using a 152-mm (6-in.) wide by 2.44-m (8-ft) long open channel flume that contained an open joint with a vertical offset into the flow located 0.91 m (3 ft) from the downstream end. The width of the joint opening (gap) was set to values of 3.2, 6.4, 12.7, and 38.1 mm (1/8, 1/4, 1/2, and 1 1/2 in.), and the size of the vertical offset was set to 3.2, 6.4, 19.1, and 38.1 mm (1/8, 1/4, 3/4, and 1 1/2 in.). In photos, the flume appears to be level, but the exact slope is undocumented. Flow was provided through an adjustable vertical slide gate that allowed the flow velocity at the offset to be varied from 2.29 to 4.57 m/s (7.5 to 15 ft/s), as measured by a Pitot tube (presumably positioned upstream from the offset joint). The open joint allowed water to enter a chamber beneath the flume that was tightly sealed. Pressures in this chamber were measured using a dynamic pressure transducer whose output was recorded on a strip chart. The joints studied were all oriented normal to the bed of the flume and extended perpendicular to the flow direction across the full width of the flume.

Average pressure values and a value that exceeded 95% of the instantaneous dynamic pressures were both determined from the strip chart records. The latter was arbitrarily selected as a value representative of maximum uplift pressures at a spillway slab. Net uplift pressure heads were reported as the difference between the high pressure in the chamber and the average depth of flow measured over the joint, but separate pressure and depth measurements were not reported. Uplift pressure heads were presented as dimensionless percentages of the computed velocity head corresponding to the average flow velocity in the channel for each test, but the data were not analyzed using any dimensionless measure of the offset heights and gap widths. Also, although the discussion suggested that uplift pressures should be related to the conditions in the boundary layer and that trends in observed uplift in the experiments were consistent with this idea, no attempt was made to quantitatively relate the uplift pressures to boundary layer velocities instead of the channel-average velocity. Boundary layer characteristics were not measured during the experiments, nor were any attempts made to analytically estimate the boundary layer conditions of the tests.

Notable trends observed in the data were:

- Uplift pressures increased with smaller gap widths. This was attributed to larger gaps allowing larger or stronger flow circulation cells to develop within the gap, dissipating some of the flow energy and reducing the uplift pressure transmitted through the gap. Another explanation is that a larger portion of the gap width was exposed to pressures below the stagnation pressure, since true stagnation of the flow only occurs at the face of the offset.
- Uplift pressures increased for larger vertical offsets, most rapidly when vertical offsets were small. At large vertical offset heights, the uplift pressure tended to approach a constant percentage of the velocity head.

- For higher velocities, the uplift pressures tended to be a slightly smaller percentage of the channel-average velocity head.

Specific flow depths, discharges, and channel slope data for each test were not reported. However, the short distance from the entrance of the flume to the joint location suggests that the boundary layer in these tests was relatively thin.

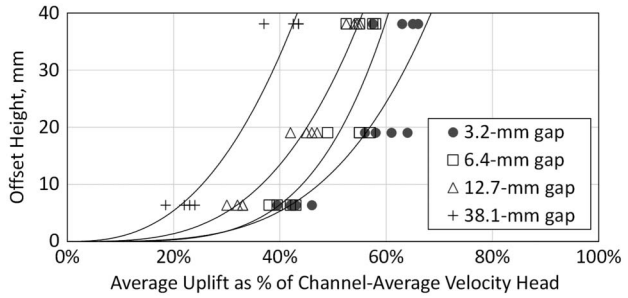

Fig. 3. Johnson (1976) data on uplift pressures in sealed offset joints, as originally presented in the form of percentages of channel-average velocity head versus offset height. Power curve trend lines for each gap width are for illustration only. Johnson (1976) drew individual curves by hand through the data points for each gap width and velocity setting.

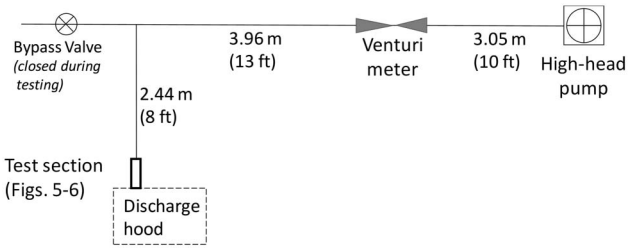

Fig. 4. Plan view of test facility setup showing pump, piping, flow meter, and test section. The 2.44-m (8-ft)–long approach to the test section consisted of a 0.91-m (3-ft)–long round-to-square transition [191-mm (7.5-in.) diameter to 102-mm (4-in.) square], followed by 1.52 m (5 ft) of 102-mm (4-in.) square duct. (Adapted from Frizell 2007.)

Fig. 3 shows Johnson's (1976) measurements of average uplift pressures in a format that is condensed but similar to the way they were first presented by Johnson. Uplift pressures are made dimensionless by expressing them as a percentage of the channel-average velocity head. Johnson originally showed data for each gap width on a separate plot, with individual hand-drawn curves passing through the data points collected at each velocity setting. In this condensed presentation, Fig. 3 shows power curves through the data for each gap width to illustrate general trends in the data. Johnson's observations highlighted previously are apparent, especially the significant increase in uplift pressure as the width of the joint gap was reduced. Although the data are not included here, trends in the 95% maximum uplift pressure data were similar, with the 95% maximum uplift typically about 1.15–1.40 times the average uplift.

Water Tunnel Tests

The second significant study of the uplift pressure phenomenon was conducted at Reclamation by the second author (Frizell 2007) using a high-head pump to deliver high-velocity flow to a pressurized water tunnel containing an idealized spillway joint that could be adjusted to create offset heights of 3.2, 6.4, 12.7, and 19.1 mm (1/8, 1/4, 1/2, and 3/4 in.) and gap widths of 3.2, 6.4, and 12.7 mm (1/8, 1/4, and 1/2 in.). The layout of the test facility is shown in Fig. 4, with the test section located downstream from a tee on the pump discharge line. The tests could be conducted with flow velocities of about 5.2–14.6 m/s (17–48 ft/s) in the 102-m-wide by 102-mm-tall (4-in. by 4-in.) section approaching the offset (Fig. 5). The exit height of the test section was reduced from the nominal 102-mm (4-in.) dimension by the height of the offset. In addition to the tests with rectangular sharp-edged joint geometries, tests were also performed on joint openings with 3.2 × 3.2-mm (1/8 × 1/8-in.) 45° chamfered edges and 3.2-mm (1/8-in.) radius edges. Tests were conducted in a sealed configuration, where no flow could exit the chamber beneath the spillway joint, and a vented condition in which flow could exit through a valve. The size of the exit valve was not reported, but its flow capacity was not enough to keep the chamber fully vented. As a result, back-pressure existed below the spillway joint in the vented tests, but it was not directly measured. Uplift pressures were measured with a differential pressure transducer connected to taps above and below the movable downstream block (Fig. 6). Particle image velocimetry

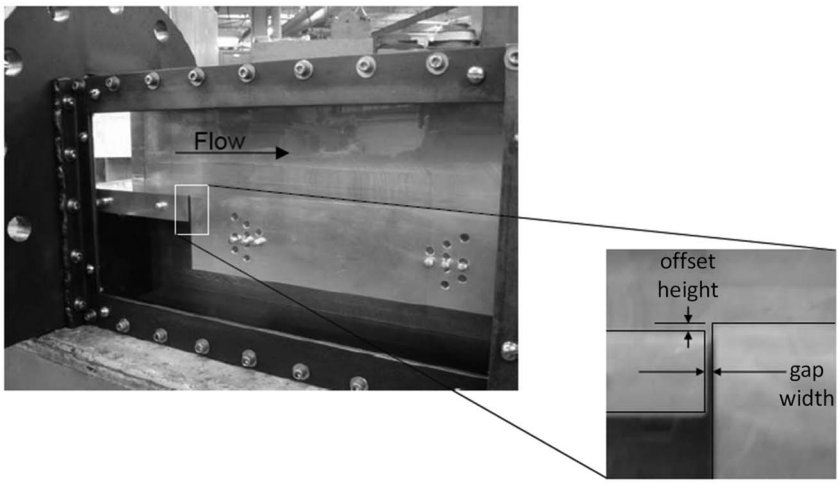

Fig. 5. Test chamber used by Frizell (2007). The upstream round-to-square transition is not yet attached. The thickness of the upstream slab is 25.4 mm (1 in.). (Adapted from Frizell 2007.)

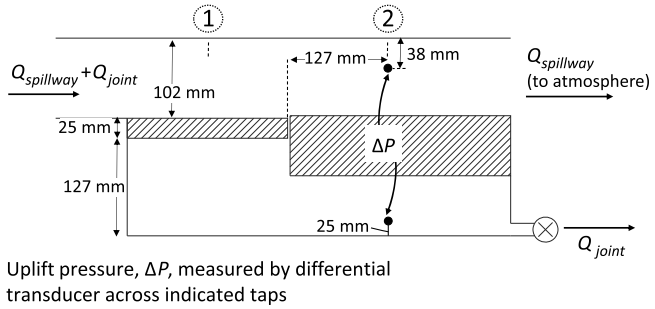

Fig. 6. Test apparatus and location of pressure taps for uplift pressure measurement. (Adapted from Frizell 2007.)

(PIV) was also used to map velocity fields above and within the joint for a small subset of the tests [chamfer-edged joints with 3-mm (1/8-in.) and 13-mm (1/2-in.) gap widths and 13-mm (1/2-in.) offset heights]. Finally, accompanying computational fluid dynamics (CFD) models were configured and run using the FLOW-3D software package developed by Flow Science. CFD models were created to simulate both the test facility and a prototype spillway joint. The PIV measurements and CFD models were used primarily to visualize the flow field in the vicinity of the joints. There is potential for CFD studies to be used to study uplift pressures, but quantitative uplift pressure results were not provided in this study.

The collected uplift pressure data were originally presented by Frizell (2007) in plots showing the raw differential pressures versus the average velocity over the offset (at Section 2 in Fig. 6). These plots verified that uplift pressure was proportional to the square of the velocity and that uplift pressures also increased with increasing offset height, but the data were not presented in a dimensionless manner that would allow direct comparison to the Johnson (1976) results. The uplift pressures tended to decrease in most cases with increasing gap widths, similar to the observation by Johnson (1976). Frizell (2007) also observed that boundary layer effects could have a substantial impact in a prototype, but made no analysis of the boundary layer conditions that existed in the tests, presuming that the boundary layer was thin and that uplift pressures would be related to mean velocities. The tests of chamfered-edged and radius-edged joint openings showed similar trends as the tests of sharp-edged openings, with a tendency for the chamfered- and radius-edged openings to behave like sharp-edged openings of a slightly larger dimension.

In the water tunnel experiments Frizell (2007) employed a differential pressure transducer connected to piezometer taps below and above the downstream slab, and reported differential pressure as the uplift pressure. However, the use of the water tunnel causes three effects that distort this measure of uplift pressure. First, there is an increase in velocity head from the section upstream from the joint (Section 1 in Fig. 6) to the section downstream from the offset (Section 2) due to the reduced height of the tunnel caused by the vertical offset. The lower velocity head at Section 1 will be accompanied by a higher pressure head than that at Section 2. The pressure in the sealed chamber beneath the slot should be expected to reflect this larger pressure head. Second, there is a loss of head at the offset due to the minor loss created by the contraction itself. This also causes an increase in pressure at Section 1. Finally, there is also a friction loss in the water tunnel that creates an additional pressure difference between the two sections. Each of these three pressure difference contributors must be subtracted from the measured pressure difference to determine the uplift caused by the stagnation of flow against the face of the vertical offset.

Similar head losses and flow changes occur in open channel flow, but they affect the uplift pressure beneath the slab differently. In the supercritical flows tested by Johnson (1976), there was an increase in depth in the downstream direction as the flow passed over the offset and experienced contraction and friction losses. (In subcritical flow, the depth decreases in the downstream direction because of friction and contraction losses and the step-up in the channel bottom). However, there was no way for this depth increase to affect the flow upstream from the face of the offset or the uplift generated by the step, since pressure waves cannot travel upstream in supercritical flow. The conditions in the sealed chamber could only be influenced by the flow upstream from the offset. The increased downstream depth did have a small effect on the pressure above the downstream slab. Although Johnson (1976) explained that he subtracted out the flow depth when reporting the net uplift pressures, he did not definitely state whether he measured the flow depth upstream or downstream from the offset. It is presumed that the measurement was made downstream from the offset, since uplift of the downstream slab was of interest, but the difference in either case would be small [probably less than 25 mm (1 in.)].

In the water tunnel configuration, the head losses and pressure changes associated with pressurized flow are substantial in comparison with the measured differential pressure heads. Unfortunately, there were no actual measurements of these head losses or the total head losses made during the tests. Therefore, estimates of each loss were calculated during the present review, and these were used to compute adjusted values of uplift pressure head that could be compared directly with the open channel data from Johnson (1976). The velocity head change was the most readily and accurately estimated, based on cross-sectional dimensions and offset height, and varied from about 14% to 50% of the measured differential pressure head. The contraction loss was estimated from equations for computing minor losses at abrupt concentric pipe contractions (Roberson and Crowe 1985) and ranged from 3% to 14% of the measured differential pressure head. The friction loss estimates had significant uncertainty depending on the assumed values of surface roughness in the test section, but were smaller than the other two effects, ranging from about 2% to 6% of the measured differential pressure head. The combined effects of all three components ranged from 20% to 66% of the measured differential pressure head.

Flow through Joints

The Frizell (2007) study reported flow rates through the joints in a vented condition, but a review of the data and the analysis procedures now shows that the pressure measurements used to indirectly determine the discharges did not accurately reflect actual flow rates. Future tests of flow through open joints should use calibrated direct flow measurements and include measurements of the back-pressure beneath the open joint. Running tests in a fully vented condition (with a much larger outlet valve) will provide an indication of the maximum flow that can occur through a joint experiencing no back-pressure from the underlying foundation or drainage system.

Analysis

The IFT (2018) approach to estimating uplift pressure head for the Oroville Dam spillway was to estimate the velocity profile in the channel—specifically, the velocity occurring at a distance above the channel bed equal to half the height of an offset into the flow. The uplift pressure was then equal to the velocity head at this point in the profile. The two experimental data sets from Johnson (1976) and Frizell (2007) offer an opportunity to test this concept, but

since velocity profiles were not measured in either study, the midheight velocity must be estimated by analytical means.

In the Johnson (1976) open channel experiments, it was reasonable to assume that the development of the boundary layer began at the slide gate that controlled the inflow, which was 1.52 m (5 ft) upstream from the simulated joint. For the Frizell (2007) water tunnel experiments, the boundary layer development was assumed to begin at the upstream end of the square duct leading to the test section, which was 1.72 m (5.66 ft) upstream from the simulated joint. [The velocity was rapidly accelerating in the round-to-square transition leading to the square duct, almost tripling in a distance of 0.91 m (3 ft).] For both cases, the velocity profile in the boundary layer can be estimated [Roberson and Crowe 1985, Eqs. (9)–(27)] as

$$v_y = u_*\left(5.75\log_{10}\frac{yu_*}{\nu} + 5.56\right) \tag{3}$$

where u_* = shear velocity; and ν = kinematic viscosity of the fluid. In the early phase of boundary layer growth, the value of u_* is a function of distance from the point of boundary layer initiation and is given by a set of three equations [Roberson and Crowe 1985, pp. 321–336, Eqs. (9)–(19) and (9)–(42)] as

$$u_* = \sqrt{\frac{\tau_0}{\rho}} \tag{4}$$

$$\tau_0 = \frac{0.058}{\sqrt[5]{\mathrm{R}_x}}\frac{\rho V^2}{2} \tag{5}$$

$$\mathrm{R}_x = \frac{Vx}{\nu} \tag{6}$$

where ρ = fluid density; V = mean channel velocity (free-stream velocity outside of the boundary layer); and x = distance from the start of boundary layer growth. This yields a straightforward way to calculate the boundary layer velocity profile as a function of mean velocity of the flow. In addition, the thickness of the boundary layer at distance x can be estimated from [Roberson and Crowe 1985, Eqs. (9)–(41)] as

$$\delta = \frac{0.37x}{\sqrt[5]{\mathrm{R}_x}} \tag{7}$$

Applying Eq. (7) to the Johnson (1976) tests, the boundary layer thickness at the test location varied from about 24.4 to 27.9 mm (0.96 to 1.1 in.), decreasing with increasing velocity. Therefore, the 38.1-mm (1.5-in.) offsets would have extended into the free-stream flow; however, offsets of 19.1 mm (0.75 in.) or less would have been fully contained in the boundary layer. For the Frizell (2007) tests, the boundary layer thickness varied from about 21.4 to 26.1 mm (0.84 to 1.03 in.), which is larger than all tested offset heights.

Johnson (1976) analyzed the uplift pressure head as a dimensionless percentage of the mean channel velocity head, but related it to dimensional offset heights and gap widths of the tested joints. Frizell (2007) plotted dimensional uplift pressure head versus mean flow velocity for different offset heights and gap widths. To generalize the results in a more useful way, Fig. 7 presents both sets of data plotted in a fully dimensionless way. This figure includes data for all gap widths, offset heights, and velocities tested by Johnson (1976) and all sealed-cavity, sharp-edged joint tests conducted by Frizell (2007). The average uplift pressure heads are presented as percentages of stagnation pressure computed for the estimated boundary layer velocity at midheight of the offset, computed using

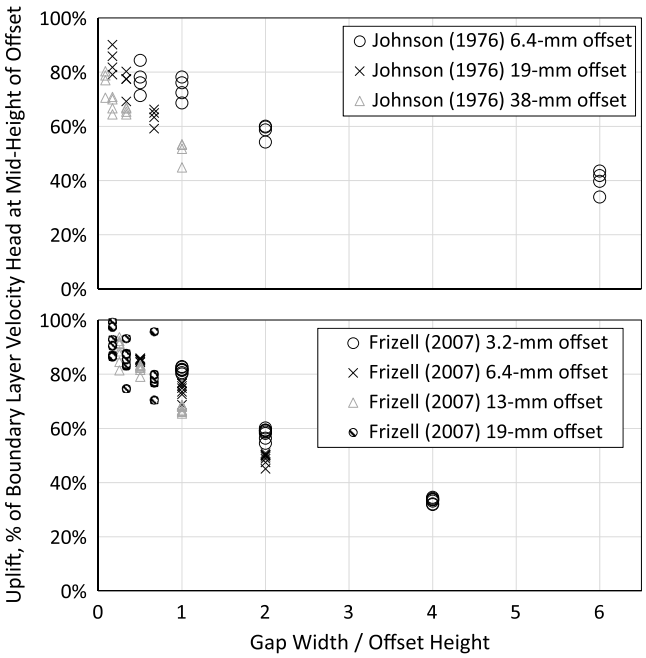

Fig. 7. Uplift pressure head as a percentage of boundary layer velocity head related to joint geometry.

Eqs. (3)–(6). Dimensionless uplift pressures are plotted as a function of the dimensionless ratio of gap width to offset height, with the data subdivided by distinct values of offset height. This presentation collapses the data more effectively than Fig. 3, indicating that uplift pressures approach 100% of the midheight boundary layer velocity head as the ratio of gap width to offset height is reduced toward zero. The plots show clearly that there is a reduction in the developed uplift pressure for relatively wide gap ratios, in contrast to the IFT (2018) assumption that the uplift pressure would be equal to the velocity head at midheight of the offset, independent of the gap width dimension. The plots show that there was some dependence in the experiments on the dimensional offset height, with the data following somewhat higher curves for smaller offsets, especially the open channel data. In general, the water tunnel data exhibit slightly larger dimensionless uplift values at low gap–offset ratios and smaller values at high ratios. These differences may be due to several factors, including viscous (Reynolds) scale effects, uncertainties in the estimates of boundary layer velocity profiles, or uncertainties related to the uplift pressure adjustments applied to the water tunnel data. A curve fit to the combined data from both studies (Fig. 8) produces Eq. (8) with an R^2 value of 0.68, which can be used to predict the uplift pressure head

$$\frac{H_u}{V_{bl}^2/(2g)} = e^{0.055-0.417\sqrt{\beta}} \tag{8}$$

where H_u = uplift pressure head; V_{bl} = boundary layer velocity mid-height of the offset; and β = gap width–offset height ratio.

In Fig. 9 uplift pressures are presented in a different dimensionless manner, as percentages of the velocity head computed from the channel-average velocity approaching the simulated joint. This collapses the data from each study into a single curve for all tested gap widths and offset heights. In Fig. 10, the data sets are combined and a single curve fit equation is obtained with an R^2 value of 0.90:

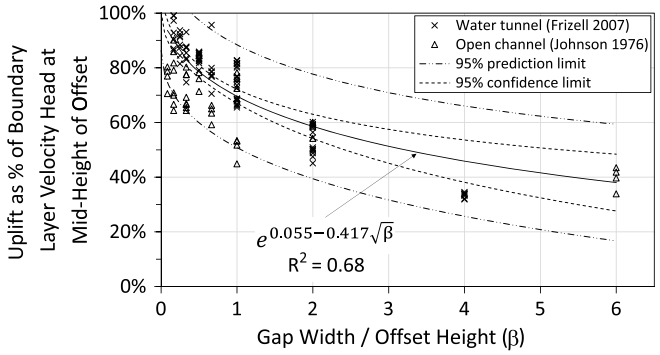

Fig. 8. Curve relating uplift pressure head to boundary layer velocity and the gap width to offset height ratio.

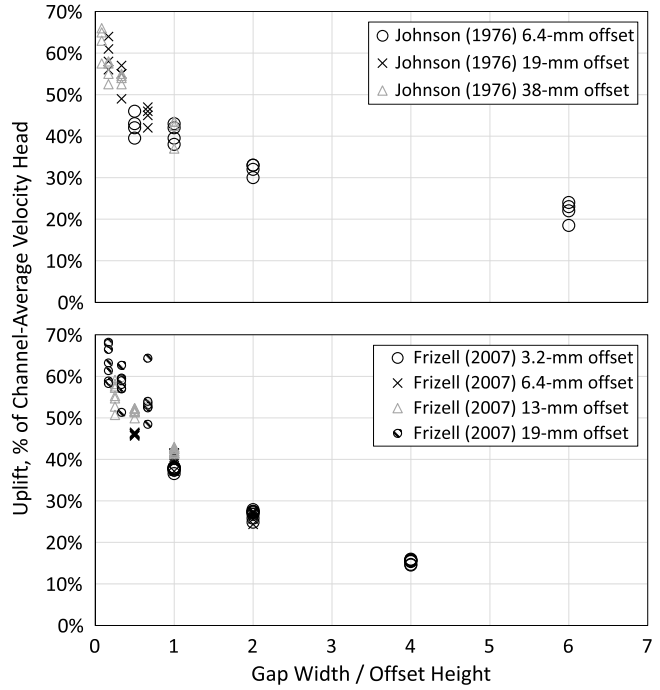

Fig. 9. Uplift pressure head as a percentage of mean channel velocity head, related to joint geometry.

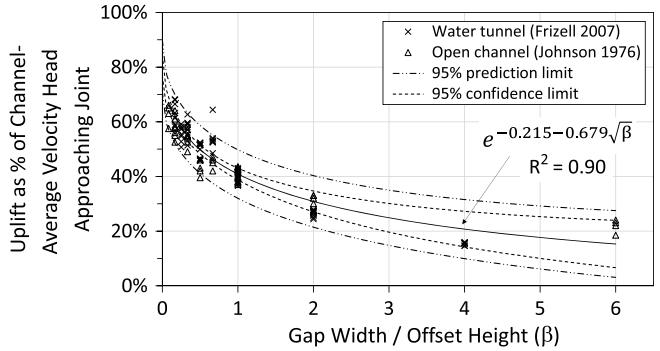

Fig. 10. Curve relating uplift pressure head to channel-mean velocity and the gap width–offset height ratio.

$$\frac{H_u}{V^2/(2g)} = e^{-0.215-0.679\sqrt{\beta}} \tag{9}$$

The variables here are the same as in Eq. (8), except that V is the average velocity for the full channel. There is still a tendency at large gap width–offset height ratios for larger uplift pressures in the open channel data, but at low gap–offset ratios the data sets coincide well. The better curve fit suggests that the actual boundary layer in both experiments may have been thinner than the calculated estimates, meaning that the uplift pressures were driven primarily by the mean channel velocity. Eq. (9) offers a useful approach to predicting uplift pressure when there is little or no boundary layer, and is more straightforward to apply than Eq. (8) since it requires determination only of the average channel velocity instead of the more complex boundary layer velocity profile. Notably, for gap width–offset height ratios less than 0.5 the uplift pressure predicted by Eq. (9) is more than 50% of the channel-average velocity head, which exceeds the estimates of uplift pressure made by the IFT (2018) for the Oroville Dam spillway (Table 1). To apply either Eq. (8) or Eq. (9) to a prototype case, the gap width–offset height ratio must be known, but the uplift pressure is not dependent on the actual offset height or gap width. In contrast, the IFT (2018) approach used the offset height but did not consider any effect of gap width. Despite these observations, one should not conclude that the magnitude of the offset height or gap width is unimportant from a practical standpoint, since large openings to the foundation should enable more flow to get beneath the slab, where it can have a myriad of undesirable affects if not captured and carried away safely. Large openings should also be expected to enable uplift pressures to extend to larger areas beneath a slab.

Scale Effects

One motivation for the water tunnel tests by Frizell (2007) was the possibility of scale effects in the low-velocity open channel tests of Johnson (1976). Low velocities and Reynolds numbers might affect turbulence intensity and boundary layer development, which could in turn affect generated uplift pressures. If Reynolds number effects were present in the laboratory tests, they should be visible in a comparison of model results obtained at different Reynolds numbers. Three possible formulations of the Reynolds number could be relevant to this flow situation. The boundary layer Reynolds number is typically defined as $\mathrm{R}_x = Vx/\nu$ [Eq. (6)], where V is the mean velocity in the channel and x is the length of the boundary layer from the start of its growth. The two other potentially useful Reynolds numbers are $\mathrm{R}_w = Vw/\nu$, where w is the gap width, and $\mathrm{R}_h = Vh/\nu$, where h is the offset height.

Frizell (2007) was able to test at velocities up to three times higher than those used by Johnson (1976), but the range of gap and offset Reynolds numbers for the two studies was similar, since Johnson (1976) tested larger gap widths and offsets. To test for Reynolds number effects, the data for each study were grouped within low, middle, and high ranges of the three Reynolds numbers, and plots like those in Figs. 7 and 9 were constructed to see if different ranges of Reynolds numbers produced different curves. No consistent Reynolds number effects could be identified that were distinct from the scatter in the data.

Application and Research Needs

The Oroville Dam Independent Forensic Team did not use the results of either the Johnson (1976) or the Frizell (2007) study for prediction of uplift pressures, instead opting to assume that uplift

would be equal to stagnation pressures associated with flow velocity in the boundary layer at midheight of an offset. The present study reanalyzed the Johnson (1976) and Frizell (2007) data sets to develop Eq. (8), which relates uplift pressure to the boundary layer velocity profile, and Eq. (9), which relates uplift pressure to mean velocity in a channel. Notably, both equations show that there is an important additional effect beyond that assumed by IFT (2018)—namely, the influence of the geometric ratio of gap width to offset height. Eq. (9) is convenient because it does not require estimation of boundary layer velocities. Both equations are superior to the relations provided by the original studies, since they use dimensionless forms that do not require matching application details to a specific test run at a particular velocity, offset height, or gap width. Because Eq. (9) is based on channel-average velocity rather than boundary layer velocity, it is likely to yield conservatively high estimates of uplift pressure for long chutes in which boundary layer velocities could be much lower than average velocities.

The uncertainty of Eq. (8) is significant, but it is still potentially valuable in prototype spillways with long chutes, since boundary layer effects could reduce uplift pressures significantly. Through its influence on the boundary layer, spillway surface roughness could be an important factor, with uniformly rough surfaces having less uplift potential than smooth surfaces. To further improve this approach to the problem, experimental data are needed from test facilities in which the boundary layer velocities are significantly different from the channel-average velocity and can be adjusted and measured. Both Johnson (1976) and Frizell (2007) varied the average flow velocity significantly, but boundary layer velocities were not measured, and estimated boundary layer velocities at midheight of the tested offsets were typically about 70%–90% of average velocity. For comparison, the Oroville Dam spillway's estimated boundary layer velocities underlying the stagnation pressure estimates in Table 1 ranged from about 50%–70% of average velocity.

Aerated flow is another factor that could have an important influence, both for its effect on the boundary layer and for its effect on pressure propagation through joints and resonance within joints. Aeration effects should be studied after nonaerated conditions are well understood.

This study has considered only the uplift pressures generated beneath a slab when the foundation is sealed. In real spillways, the natural or engineered methods for conveying water out of the foundation and dissipating uplift pressure are also important for determining total uplift forces. To assess the removal of water from the foundation, it is necessary to estimate amounts of water entering through spillway joints or cracks. For this purpose, IFT (2018) used equations that predicted leakage rates due to piezometric pressure heads in the chute (i.e., pressure due only to depth of flow); these equations did not reflect any increased flow that might occur because of an offset projecting into the flow. Currently there is no good source of laboratory testing to support making estimates of flow through joints with offsets. Research should be initially focused on prediction of flow rates assuming fully vented conditions beneath the slab or partially vented conditions with measurement of back-pressure beneath the slab. For application in the field, flow rates estimated for the fully vented condition could be modified based on a separate analysis of the underlying drainage layer or drainage system.

A potentially valuable avenue for further research on this topic is field-scale studies. To the best of the authors' knowledge, there have been no attempts to measure uplift pressures beneath the lining of prototype spillways. An instrumented prototype spillway could enable the collection of data for high-velocity flows with realistic boundary layer and aerated flow conditions.

This review was initiated with the goal of developing a research plan to address the influence of factors such as complex flow paths through spillway joints (effects of keyways, waterstops, reinforcement, etc.), variations in joint openness, and differences in joint configuration (vertical offsets, spalls, and joints oriented acutely to the flow). However, it has shown that there are still fundamental issues that need to be resolved before these complexities are considered. Until the necessary research can be completed, defensive design practices and proactive maintenance programs to prevent the widespread existence of open or offset joints are crucial to defend against hydraulic jacking.

Acknowledgments

The authors appreciate the detailed comments of the three anonymous reviewers and the editor and associate editor. Their constructive criticism led to significant improvement in the paper. The data from Johnson (1976) were digitized from the original figures and can be obtained by email request from the lead author, along with the complete data set from the Frizell (2007) study. The authors wish to especially acknowledge the work of the late Perry Johnson, who inspired us all and continues to do so today. This work was jointly funded by Reclamation's Science & Technology Program and Dam Safety Technology Development Program.

Notation

The following symbols are used in this paper:

e = base of natural logarithms, 2.7183;
f = Darcy-Weisbach friction factor;
g = acceleration due to gravity;
H_u = uplift pressure head;
h = offset height;
P_s = stagnation pressure;
Q_{joint} = flow rate through spillway joint;
Q_{spillway} = flow over slab downstream from offset joint;
Q_{total} = total flow approaching offset in water tunnel test facility;
R_x = boundary layer Reynolds number based on mean velocity and distance from start of boundary layer growth, $\mathsf{R}_x = Vx/\nu$;
R_w = Reynolds number based on mean velocity and gap width, $\mathsf{R}_w = Vw/\nu$;
R_h = Reynolds number based on mean velocity and offset height, $\mathsf{R}_h = Vh/\nu$;
V = mean flow velocity approaching spillway joint;
V_{bl} = boundary layer velocity mid-height of an offset;
u_* = shear velocity;
v_y = velocity at distance y above boundary; approach velocity of stagnated flow;
w = gap width;
x = distance from start of boundary layer growth;
y = distance from boundary;
y_0 = total flow depth;
β = ratio of gap width to offset height;
γ = unit weight of water;
ΔP = pressure difference between chamber below slab and water tunnel flow above slab;
δ = boundary layer thickness;

ν = kinematic viscosity;
ρ = fluid density; and
τ_0 = bed shear stress.

References

Barjastehmaleki, S., V. Fiorotto, and E. Caroni. 2016a. "Design of stilling basin linings with sealed and unsealed joints." *J. Hydr. Eng.* 142 (12): 04016064. https://doi.org/10.1061/(ASCE)HY.1943-7900.0001218.

Barjastehmaleki, S., V. Fiorotto, and E. Caroni. 2016b. "Spillway stilling basins lining design via Taylor hypothesis." *J. Hydr. Eng.* 142 (6): 04016010. https://doi.org/10.1061/(ASCE)HY.1943-7900.0001133.

Bellin, A., and V. Fiorotto. 1995. "Direct dynamic force measurement on slabs in spillway stilling basins." *J. Hydr. Eng.* 121 (10): 686–693. https://doi.org/10.1061/(ASCE)0733-9429(1995)121:10(686).

Bollaert, E., and A. Schleiss. 2003a. "Scour of rock due to the impact of plunging high velocity jets. I: A state-of-the-art review." *J. Hydr. Res.* 41 (5): 451–464. https://doi.org/10.1080/00221680309499991.

Bollaert, E., and A. Schleiss. 2003b. "Scour of rock due to the impact of plunging high velocity jets. II: Experimental results of dynamic pressures at pool bottoms and in one- and two-dimensional closed end rock joints." *J. Hydr. Res.* 41 (5): 465–480. https://doi.org/10.1080/00221680309499992.

Bollaert, E., and A. Schleiss. 2005. "Physically based model for evaluation of rock scour due to high-velocity jet impact." *J. Hydr. Eng.* 131 (3): 153–165. https://doi.org/10.1061/(ASCE)0733-9429(2005)131:3(153).

Bowers, C. E., and J. Toso. 1988. "Karnafuli Project, model studies of spillway damage." *J. Hydr. Eng.* 114 (5): 469–483. https://doi.org/10.1061/(ASCE)0733-9429(1988)114:5(469).

Bureau of Reclamation. 2014. "General spillway design considerations." Chap. 3 in Reclamation: Managing water in the West. Design standards No. 14, appurtenant structures for dams (spillways and outlet works). Accessed January 16, 2019. https://www.usbr.gov/tsc/techreferences/designstandards-datacollectionguides/finalds-pdfs/DS14-3.pdf.

Dong, Z., Y. Wu, and D. Zhang. 2010. "Cavitation characteristics of offset-into-flow and effect of aeration." *J. Hydr. Res.* 48 (1): 74–80. https://doi.org/10.1080/00221680903566083.

Falvey, H. T. 1990. *Cavitation in Chutes and spillways. Engineering monograph 42*. Denver: US Dept. of the Interior, Bureau of Reclamation.

Fiorotto, V., and E. Caroni. 2014. "Unsteady seepage applied to lining design in stilling basins." *J. Hydr. Eng.* 140 (7): 04014025. https://doi.org/10.1061/(ASCE)HY.1943-7900.0000867.

Fiorotto, V., and A. Rinaldo. 1992a. "Fluctuating uplift and lining design in spillway stilling basins." *J. Hydr. Eng.* 118 (4): 578–596. https://doi.org/10.1061/(ASCE)0733-9429(1992)118:4(578).

Fiorotto, V., and A. Rinaldo. 1992b. "Turbulent pressure fluctuations under hydraulic jumps." *J. Hydr. Res.* 30 (4): 499–520. https://doi.org/10.1080/00221689209498897.

Fiorotto, V., and P. Salandin. 2000. "Design of anchored slabs in stilling basins." *J. Hydr. Eng.* 126 (7): 502–512. https://doi.org/10.1061/(ASCE)0733-9429(2000)126:7(502).

Frizell, K. W. 2007. *Uplift and crack flow resulting from high velocity discharges over open offset joints*. Rep. No. DSO-07-07. Denver: Bureau of Reclamation Dam Safety Technology Development Program.

González-Betancourt, M., and L. Posada-García. 2016. "Effects of joints and their waterstops on pressures spread over a slab." *DYNA* 83 (197): 94–103. https://doi.org/10.15446/dyna.v83n197.47579.

Hepler, T. E., and P. L. Johnson. 1988. "Analysis of spillway failures by uplift pressure." In *Proc., 1988 National Conf. on Hydraulic Engineering and Int. Symp. on Model-Prototype Correlations*, edited by S. R. Abt and J. Gessler. Reston, VA: ASCE.

IFT (Independent Forensic Team). 2018. "Independent forensic team report: Oroville dam spillway incident." Accessed January 5, 2018. https://damsafety.org/sites/default/files/files/IndependentForensicTeamReportFinal01-05-18.pdf.

Johnson, P. L. 1976. "Research into uplift on steep chute lateral linings." Accessed April 18, 2018. https://www.usbr.gov/tsc/techreferences/hydraulics_lab/pubs/PAP/PAP-1163.pdf.

Liu, P. Q., and A. H. Li. 2007. "Model discussion of pressure fluctuations propagation within lining slab joints in stilling basins." *J. Hydr. Eng.* 133 (6): 618–624. https://doi.org/10.1061/(ASCE)0733-9429(2007)133:6(618).

Mahzari, M., and A. J. Schleiss. 2010. "Dynamic analysis of anchored concrete linings of plunge pools loaded by high velocity jet impacts issuing from dam spillways." *Dam Eng.* 20 (4): 307–327.

Melo, J. F., A. N. Pinheiro, and C. M. Ramos. 2006. "Forces on plunge pool slabs: influence of joints location and width." *J. Hydr. Eng.* 132 (1): 49–60. https://doi.org/10.1061/(ASCE)0733-9429(2006)132:1(49).

Pells, S. 2016. "Erosion of rock in spillways." Doctoral thesis, Univ. of New South Wales, School of Civil and Environmental Engineering.

Roberson, J. A., and C. T. Crowe. 1985. *Engineering fluid mechanics*. 3rd ed. Boston: Houghton Mifflin.

Rouse, H. 1945. *Elementary mechanics of fluids*, 199. New York: Wiley.

Toso, J. W., and C. E. Bowers. 1988. "Extreme pressures in hydraulic-jump stilling basins." *J. Hydr. Eng.* 114 (8): 829–843. https://doi.org/10.1061/(ASCE)0733-9429(1988)114:8(829).

Trojanowski, J. 2004. "Assessing failure potential of spillways on soil foundation." In *Proc., Association of State Dam Safety Officials Annual Conf.* Lexington, KY.

Trojanowski, J. 2008. "DAM SAFETY: Evaluating spillway condition." Accessed October 1, 2018. https://www.hydroworld.com/articles/hr/print/volume-27/issue-2/technical-articles/dam-safety-evaluating-spillway-condition.html.

Wahl, T. L., K. W. Frizell, and H. T. Falvey. 2019. *SpillwayPro—Tools for analysis of spillway cavitation and design of Chute Aerators*. Hydraulic Laboratory Rep. No. HL-2019-03. Denver: US Dept. of the Interior, Bureau of Reclamation.